Claudin-1 enhances chemoresistance of human lung adenocarcinoma A549 cells mediated by forming an amino acid barrier

Riho Kimura
Gifu Pharmaceutical University
Ayaka Ito
Gifu Pharmaceutical University
Shotaro Hashimoto
Gifu Pharmaceutical University
Hiroaki Eguchi
Gifu Pharmaceutical University
Haruka Nasako
Gifu Pharmaceutical University
Yui Takashina
Gifu Pharmaceutical University
Yoshifumi Morikawa
Gifu Prefectural Police Headquarters
Koichi Suenami
Gifu Prefectural Police Headquarters
Yuta Yoshino
Gifu Pharmaceutical University
Satoshi Endo
Gifu Pharmaceutical University
Toshiyuki Matsunaga
Gifu Pharmaceutical University
Akira Ikari
ikari@gifu-pu.ac.jp

Gifu Pharmaceutical University

Article

Keywords: claudin-1, amino acid transport, chemoresistance

Posted Date: March 5th, 2024

DOI: https://doi.org/10.21203/rs.3.rs-3968542/v1

Additional Declarations: No competing interests reported.

Abstract

Claudin-1 (CLDN1) is highly expressed in human lung adenocarcinoma-derived A549 cells and is involved in the augmentation of chemoresistance. However, the mechanism of chemoresistance is not fully understood. In the tumor microenvironment, cancer cells are exposed to stress conditions such as hypoxia and malnutrition. Here, we investigated the effect of CLDN1 expression on amino acid (AA) flux and chemoresistance using A549 cells. L-type AA transporters, LAT1 and LAT3, were highly expressed in three-dimensional spheroid cells compared with in two-dimensional (2D) cultured cells. The expression of these transporters was increased by AA deprivation in 2D cultured cells. The paracellular AA flux except for Ser, Thr, and Tyr was enhanced by CLDN1 silencing. The expression of AA transporters and AA contents in spheroids were decreased by CLDN1 silencing. These results suggest that CLDN1 forms a paracellular AA barrier, leading to a compensatory increase in LAT1/3 expression in spheroids. The production of reactive oxygen species in the mitochondria and cytosol was decreased by CLDN1 silencing in spheroids, resulting in downregulation of the expression of nuclear factor erythroid 2-related factor 2 (Nrf2) and its target antioxidant genes. CLDN1 silencing enhanced the cytotoxicity of doxorubicin, an anthracycline antitumor agent, which was blocked by sulforaphane, an Nrf2 activator. In 2D cultured cells, the cytotoxicity of doxorubicin was attenuated by a reduction in extracellular AA concentration or treatment with sulforaphane. We suggest that CLDN1 forms an AA barrier in spheroids, leading to the augmentation of Nrf2-dependent chemoresistance in A549 cells.

1. Introduction

Malignant transformation of cancer is a major problem in cancer treatment. Solid cancer cells form a microenvironment in the body. The microenvironment is composed of malignant, nonmalignant, and immune cells, and other constituents [1]. Vascular endothelial cells make immature and inefficient blood vessels, leading to hypoxia, malnutrition, and elevated reactive oxygen species (ROS) levels in the tumor microenvironment. Cancer cells may acquire chemoresistance mediated by the induction of adaptative stress-response mechanisms such as the hypoxia-induced factor-1 (HIF-1) [2] and Kelch-like ECH-associated protein 1 (Keap-1)/nuclear factor-erythroid 2-related factor 2 (Nrf2) pathways [3]. However, the stress formation mechanisms in the microenvironment remain to be fully elucidated.

Epithelial cells establish tight junctions (TJs) at the lateral membrane between neighboring cells [4]. TJs form continuous strands that exhibit a belt-like network. TJ strands are composed of integral membrane proteins linked with cytoplasmic scaffolding proteins such as zonula occludens-1 (ZO-1) and ZO-2. Claudins (CLDNs) are one of the major integral membrane proteins of TJs and may have pivotal roles of modulating various cellular processes such as cell proliferation, differentiation, and migration [5]. CLDNs have four transmembrane domains and two extracellular loop domains with the cytosolic amino- and carboxyl-terminal domains. So far, over 20 subtypes of CLDNs have been identified in mammals [6]. Each subtype is selectively expressed in whole-body tissues and they confer specific barrier or channel properties to each cell. Some CLDNs, including CLDN1, 3, 5, 11, and 12, function as a paracellular barrier

to mineral ions [7]. CLDN2, 10b, and 15 make paracellular cationic pores, whereas CLDN7, 10a, and 17 make anionic pores. The charge selectivity of each CLDN is determined by charged amino acid (AA) sequences in the first extracellular loop domain. Paracellular ion permeability may be characterized by the combinational expression of these CLDN subtypes. CLDNs also have a barrier ability against the transport of aqueous small molecules across the epithelial membrane. This physical barrier may be formed by the second extracellular loop domain, which is involved in the trans-interaction of CLDNs [8]. However, the barrier property of each CLDN subtype is not fully understood.

Cancer cells usually have higher rates of growth, mitosis, and migration than normal cells. Therefore, it is typical to think that the expression of CLDNs is downregulated in cancer cells. However, many investigators reported that some CLDN types are selectively and specifically upregulated in solid tumor tissues [9,10]. The differences in CLDNs expression in cancer tissues may result from genetic heterogeneity. We reported previously that CLDN1 and CLDN2 are highly expressed in the human lung adenocarcinoma tissues and their derived A549 cells [11,12]. The silencing of CLDN1 expression by siRNA leads to an attenuation of cytotoxicity against anticancer drugs in A549 spheroids. CLDN1 may enhance chemoresistance mediated by the decrease in accumulation of anticancer drugs and/or activation of chemoresistance mechanisms. Correlations between CLDN1 expression and chemoresistance has been reported in lung squamous cell carcinoma cells [13], colorectal cancer cells [14], and liver cancer cells [15]. However, the detailed mechanisms have not yet been elucidated. We recently found that CLDN2 makes a paracellular barrier to glucose and suppresses the glycolysis pathway, leading to the elevation of ROS stress and chemoresistance in A549 cells [16]. On the other hand, CLDN1, which is highly expressed in lung adenocarcinoma cells similar to CLDN2, is not involved in the regulation of paracellular glucose flux. Therefore, it is necessary to clarify what mechanism is involved in the augmentation of chemoresistance based on CLDN1 expression.

In the present study, we found that paracellular AA flux is increased by CLDN1 silencing in A549 cells. The transport and metabolism of AAs are involved in the acquisition of chemoresistance in these cancer cells [17]. To clarify the mechanism of CLDN-induced chemoresistance, we investigated the correlation between CLDN1 expression and AA contents using two-dimensional (2D) and three-dimensional (3D) culture models. mRNA and protein expression levels were determined by quantitative real-time polymerase chain reaction (PCR) and Western blotting analyses, respectively. The paracellular barrier ability of CLDN1 was examined by transepithelial electrical resistance (TER) and the fluxes of glucose and AAs. The cytotoxicity of anticancer drugs in spheroids was estimated by measuring ATP content. This is the first report showing that CLDN1 can augment chemoresistance mediated by a restriction of AA supply in spheroids of lung adenocarcinoma A549 cells.

2. Results

2.1. Expression of AA transporters in 2D and 3D cultured A549 cells

The mRNA and protein levels of AA transporters were investigated by quantitative real-time PCR and Western blotting, respectively, using 2D and 3D cultured A549 cells. The mRNA levels of LAT1, LAT2, and LAT3 in 3D spheroids were higher than those in 2D adhesion cells (Fig. 1A). The protein levels of LAT1 and LAT3 showed a similar correlation between 2D and 3D spheroids (Fig. 1B). In contrast, the protein levels of LAT2 showed the opposite change. The disparities between the mRNA and protein expression levels of LAT2 may reflect translational and/or post-translational regulation.

2.2. Effects of stress conditions on the expression of AA transporters in 2D cultured A549 cells

The tumor microenvironment forms stress conditions such as hypoxia and malnutrition. The exposure of 2D cultured A549 cells to hypoxia induces a decrease in the mRNA level of LAT3 without affecting those of LAT1 and LAT3 (Fig. 2A). The mRNA levels of LAT1, LAT2, and LAT3 were unchanged by treatments with a high concentration of lactate, an endo-product of glycolysis pathway, and glucose depletion. In contrast, both the mRNA levels of LAT1 and LAT3 were significantly increased by AA depletion without affecting that of LAT2. Similarly, the protein levels of LAT1 and LAT3 were increased by a reduction in AA concentration in the culture media (Fig. 2B). These results indicate that both the expression levels of LAT1 and LAT3 were sensitive to extracellular AA concentration.

2.3. Effects of CLDN1 and CLDN2 silencing on paracellular permeability

Both CLDN1 and CLDN2 are highly expressed in human lung adenocarcinoma tissues and A549 cells [11,12]. The barrier function of CLDN1 and CLDN2 was estimated by TER and paracellular fluxes of AA and glucose using A549 cells cultured on transwell plates. TER was increased by CLDN2 silencing (Fig. 3A), which may because of the decrease in pore-forming CLDN2 expression. In contrast, TER was unchanged by CLDN1 silencing. The paracellular AA (Mw: 75–204) and glucose (Mw: 180) fluxes were increased by CLDN1 and CLDN2 silencing, respectively (Fig. 3B). Liquid chromatography-mass spectrometry analysis showed that the fluxes of 13 AAs were detected in our experimental conditions, and CLDN1 silencing increased the fluxes of most of AAs except for Ser, Thr, and Tyr (Fig. 3C). These results indicate that CLDN1 may function as AA barrier in A549 cells.

2.4. Effects of CLDN1 silencing in spheroids on LAT expression and AA content

CLDN1 expression in spheroids was silencing by siRNA targeting CLDN1 (Fig. 4A). Electron microscopy analysis revealed that the formation of membrane fusions (so-called kissing point) was detected on the outer layer of spheroids, which was decreased by CLDN1 silencing (Fig. 4B). After treating spheroids with CytoVista 3D Cell Culture Clearing Reagent, the distribution of CLDN1 protein in spheroids was investigated using immunofluorescence analysis. The red signal of CLDN1 was mainly detected in the

outer layer of spheroids, which was decreased by CLDN1 silencing (Fig. 4C). The AA contents and mRNA levels of LAT1 and LAT3 in spheroids were decreased by CLDN1 silencing (Fig. 4D and 4E). The correlation between AA concentration and LAT expression is similar to the results in 2D cultured cells treated with AA depletion.

2.5. Effects of CLDN1 silencing in spheroids on AA metabolism

Cancer cells utilize intracellular AAs for ATP generation in the mitochondrial TCA cycle. As shown in Fig. 4E, the AA contents in spheroids were decreased by CLDN1 silencing. Therefore, there is a possibility that CLDN1 expression affects mitochondrial function. To clarify this hypothesis, we investigated mitochondrial potential and ROS generation. The fluorescence ratio of green/red of JC-1, a fluorescent indicator of mitochondrial potential, was decreased by CLDN1 silencing (Fig. 5A). CLDN1 silencing induced a reduction in the fluorescence intensities of MitoROS 580 and CellROX DeepRed (CellROX), fluorescent indicators of mitochondrial and whole cell ROS generation, respectively (Fig. 5B). These results indicate that CLDN1 may enhance oxidative stress mediated via the activation of mitochondrial function and ROS generation.

2.6. Effects of CLDN1 silencing in spheroids on Nrf2 signaling

Cytosolic Keap-1 binds to Nrf2 and restrains its signal activity through ubiquitination and proteasome-dependent degradation in control conditions. ROS promotes Keap-1 oxidization, leading to activation of Nrf2 signaling [3]. CLDN1 silencing increased the protein level of Nrf2 without affecting HIF-1α expression, a master regulator of hypoxia (Fig. 6A). The activation of Nrf2 can induce the expression of numerous genes, including antioxidant enzymes, heme oxygenase-1 (HO-1), NAD(P)H:quinone oxidoreductase-1 (NQO-1), and glutamate cysteine ligase catalytic subunit (GCLM) [18]. The mRNA expression levels of these antioxidant enzymes were deceased by CLDN1 silencing (Fig. 6B). CLDN1 silencing may diminish Nrf2 signaling in spheroids mediated by a reduction in ROS generation.

2.7. Effects of AA deficiency in a 2D culture *model on the expression of LAT and ROS generation*

As shown in Fig. 3B, CLDN1 may function as a paracellular barrier to AAs. There is a possibility that AA deficiency activates ROS generation and Nrf2 signaling [19]. To clarify the association between Nrf2 and LAT expression, we investigated the effect of halofuginone, a potent Nrf2 inhibitor. In a 2D culture model, the AA deficiency-induced elevation of LAT1 and LAT3 was inhibited by halofuginone (Fig. 7A). In addition, the AA deficiency-induced elevation of antioxidant enzymes was significantly inhibited by halofuginone. These results indicated that Nrf2 signaling and LAT1/3 expression levels are upregulated by AA deficiency.

The protein level of Nrf2 was increased by AA deficiency, whereas that of HIF-1α was not (Fig. 7B). Mitochondria play important roles in the regulation of proliferation and survival in cancer cells mediated through the maintenance of oxidative equilibrium and mitochondrial membrane potential [39]. Mitochondrial potential was increased by AA deficiency (Fig. 7C). Furthermore, both mitochondrial and cytosolic ROS contents were increased by AA deficiency. These results indicate that a restriction in AA supply may activate Nrf2 signaling mediated by the elevation of mitochondrial function and ROS generation.

2.8. Effects of AA deficiency and Nrf2 activator on doxorubicin (DXR)-induced cytotoxicity

Nrf2 is associated with the elevation of chemoresistance in numerous solid cancer cells such as lung, liver, colon, and so on [20]. DXR-induced toxicity was suppressed by sulforaphane, an inducer of Nrf2 signaling (Fig. 8A). Similarly, DXR-induced toxicity was suppressed in cells preincubated in medium containing 50% AAs (Fig. 8B). To confirm the involvement of CLDN1, we investigated the effect of CLDN1 silencing. DXR-induced toxicity was enhanced by CLDN1 silencing, which was canceled by sulforaphane (Fig. 8C). These results indicate that CLDN1 may enhance chemoresistance mediated by the restriction of AA supply and activation of Nrf2 signal. The putative scheme of CLDN1-induced chemoresistance in A549 spheroids is shown in Fig. 9.

3. Discussion

LAT1 is highly expressed in solid tumors, including lung, colon, and liver, and is associated with tumor proliferation, angiogenesis, and poor survival [21]. The 5-year survival rate of LAT1-positive patients is worse than that of LAT1-negative patients in pathological stage I of non-small cell lung cancer (NSCLC) [22]. LAT1 expression is positively associated with non-response to chemotherapy with platinum-based drugs [23]. In addition, LAT1 silencing in NSCLC cells induces the downregulation of programmed cell death 1 ligand 1, an immune checkpoint inhibitor [24]. Therefore, LAT1 is suggested to be closely associated with malignancy of NSCLC. In the present study, we found that CLDN1 expression correlated with LAT1 and LAT3 expression in A549 spheroids (Fig. 4). It is unclear whether LAT3 is associated with malignancy in NSCLC, but it is reported to be a prognosis marker for gastric [25], liver [26], and prostate cancers [27].

Inner cancer cells in the tumor microenvironment are generally exposed to malnutrition, oxidative stress, and hypoxia stress, leading to malignant transformations. LATs transport branched-chain AAs, especially leucine, into cells, resulting in the promotion of cell proliferation mediated by activation of the mammalian target of rapamycin (mTOR) pathway. Information about transcriptional regulation of LATs is limited [28]. The induction of hypoxia-induced transcriptional regulators, HIF-1 and HIF-2, upregulates LAT1 expression in human glioblastoma cells [29]. Glucose deprivation induces LAT1 expression in cultured rat retinal capillary endothelial cells [30]. We found that both LAT1 and LAT3 expression levels in

2D cultured A549 cells were increased by extracellular AA deficiency, but not by hypoxia and glucose deficiency (Fig. 2). Thus, the regulatory mechanism of LAT1 expression in A549 cells may be different from the known regulatory mechanisms. We found that AA deficiency increases ROS generation and expression of the oxidative stress response element Nrf2 (Fig. 7B). The transcription of LAT1 has been reported to be increased by activation of the Nrf2 pathway in the striatum [31]. Expression of LAT1 in A549 cells may be upregulated by the ROS-dependent Nrf2 pathway.

CLDN1 forms a paracellular barrier to aqueous small molecules [32]. The regulatory mechanisms of AA flux by CLDNs are not fully understood. We recently reported that CLDN4 and CLDN8 silencing especially enhances basic AAs and middle molecular size AAs in mouse colonic epithelial cells, respectively [33,34]. On the other hand, the current data indicate that CLDN1 silencing enhances paracellular AA flux except for Ser, Thr, and Tyr in A549 cells (Fig. 3C). The common property of these AAs is that they are neutral AAs and have a hydroxy residue. The second extracellular loop domain of CLDN1 contains more hydrophobic AAs than those in CLDN4 and CLDN8 [8]. Interaction of the second extracellular loop domain of CLDN1 and free AAs with a hydroxy residue may be weaker than that of CLDN4 and CLDN8.

CLDN1 silencing enhances sensitivity to DXR in A549 spheroids, but the mechanisms have not been clarified in detail. Our previous data indicated that CLDN1 blocks the influx of DXR into A549 spheroids [12]. Here, we found that CLDN1 may function as a paracellular barrier to AAs (Fig. 3B). mTORC1, which can be activated by extracellular AAs and growth factors, is a negative regulator of autophagy [28]. In response to the AA depletion, various cancer cells activate autophagy to overcome nutrient stress. There is a possibility that CLDN1 enhances chemoresistance mediated by the induction of autophagy because CLDN1 may block the influx of AAs into spheroids. However, this hypothesis was not supported because the AA contents in control spheroids were higher than that in CLDN1-silenced spheroids (Fig. 4E). CLDN1 silencing attenuates the expression of Nrf2 and downstream antioxidant genes (Fig. 6). DXR-induced cytotoxicity was enhanced by CLDN1 silencing in A549 spheroids, which was blocked by the Nrf2 activator sulforaphane (Fig. 8). Furthermore, DXR-induced cytotoxicity was enhanced by AA deficiency and sulforaphane treatment of 2D cultured cells. Cancer cells undergo reprogramming of glucose, fatty acid, and AA metabolism to survive and grow in stress conditions [35]. The expression of Nrf2 has been reported to be correlated with mitochondrial redox status [36]. Our data indicated that CLDN1 silencing downregulates mitochondrial ROS generation (Fig. 5B). We suggest that Nrf2 is involved in CLDN1-induced chemoresistance in A549 spheroids.

Saito *et al.* [37] reported that the cytotoxicity of gefitinib, a small-molecule epidermal growth factor receptor tyrosine kinase inhibitor, is enhanced by AA starvation in A549 cells, which is different from our results with DXR (Fig. 8B). This discrepancy may be caused by a difference in AA concentration; they used completely AA-deficient medium, whereas we used 50% AA-deficient medium. The AA content in spheroids was not completely zero regardless of whether CLDN1 was present or not (Fig. 4E). We also identified that AA starvation (0% AA) enhanced DXR-induced toxicity in A549 cells (data not shown). Our data suggest that mild deficiency of AAs induces chemoresistance in lung adenocarcinoma cells.

In conclusion, we found that both LAT1 and LAT3 expression levels were upregulated by AA deficiency in A549 cells. CLDN1 can function as a paracellular barrier to AAs except for Ser, Thr, and Tyr. The expression of LAT1 and LAT3, mitochondrial activity, ROS production, Nrf2 expression, and antioxidant enzyme expression were downregulated by CLDN1 silencing in A549 spheroids. The cytotoxicity of DXR was suppressed by extracellular AA deficiency and treatment with an Nrf2 activator. We suggest that CLDN1 enhances chemoresistance of lung adenocarcinoma cells mediated by a restriction in AA supply.

4. Material and methods

4.1. Cell culture

Human lung adenocarcinoma-derived A549 cells (RCB0098) were purchased from RIKEN BRC through the National Bio-Resource Project of the MEXT (Ibaraki, Japan). In the 2D and 3D cultures, the cells were seeded on flat-bottomed plates and PrimeSurface round-bottomed plates (Sumilon, Sumitomo, Osaka, Japan), respectively. The cells were cultured in Dulbecco's modified Eagle's medium (Sigma-Aldrich, Saint Louis, MO, USA) containing 5% fetal bovine serum, 0.07 mg/mL penicillin-G potassium, and 0.14 mg/mL streptomycin sulfate as described previously [12]. Hypoxia conditions were achieved by placing the cells in an anaerobic storage container (Anaeropack System, Mitsubishi Gas Chemical, Tokyo, Japan).

4.2. Sodium dodecyl sulfate polyacrylamide gel electrophoresis (SDS-PAGE) and Western blotting

Cell lysates were prepared as described previously [12]. The aliquots were separated by SDS-PAGE in reducing conditions and transferred to polyvinylidene fluoride membranes. After blocking with 2% skim milk, the membrane was incubated with each primary antibody overnight at 4°C. The list of primary antibodies is shown in Table 1. Then, the membrane was incubated with horseradish peroxidase-conjugated secondary antibodies for 1 h at room temperature. The protein bands were detected using EzWestLumi plus (Atto Corporation, Tokyo, Japan) or Western BLoT Chemiluminescence HRP Substrate (Takara Bio, Shiga, Japan) and visualized using a C-DiGit Blot Scanner (LI-COR Biotechnology, Lincoln, NE, USA). The band density was quantified using ImageJ software (National Institute of Health, Bethesda, MD, USA) and normalized to an internal control, β-actin.

Table 1
Primary antibodies for Western blotting and immunocytochemistry

Name	Catalog number	Supplier	Address
LAT1 (SLC7A5)	PA5-91842	Thermo Fisher Scientific	Rockford, IL, USA
LAT2 (SLC7A8)	NBP2-93913	Novus Biologicals	Easter Ave, CO, USA
LAT3 (SLC43A1)	10444-1-AP	Proteintech	Rosemont, IL, USA
CLDN1	51-9000	Thermo Fisher Scientific	Rockford, IL, USA
ZO-1	33-9100	Thermo Fisher Scientific	Rockford, IL, USA
HIF-1α	bs-0737R	Bioss Antibodies	Woburn, MA, USA
Nrf2	GTX102572	GeneTex	Irvine, CA, USA
b-Actin	sc-1615	Santa Cruz Biotechnology	Santa Cruz, CA, USA

4.3. Quantitative real-time PCR

Total RNA was extracted using TRI reagent (Molecular Research Center, Cincinnati, OH, USA) and the first strand cDNA was synthesized using a ReverTra Ace Kit (Toyobo, Osaka, Japan). mRNA expression levels were quantified using real-time PCR with real time PCR Eco (As One, Tokyo, Japan). The list of primer pairs is shown in Table 2. After normalizing to an internal control, β-actin, the relative mRNA expression was shown as a percentage of the control cells.

Table 2
Primer pairs for real-time PCR

Genes	Direction	Sequence (5'——→3')
LAT1	Sense	TGTTCACGTGTGTGATGACG
	Antisense	CAGGATGAAGAACACAGGCA
LAT2	Sense	CCTCATCGTGGAGGATGTTT
	Antisense	GCATATGCAGAACACGATGG
LAT3	Sense	TCTCCGTTGATATTCCTGGC
	Antisense	GGGAACGTAATGGCAGAAGA
HO-1	Sense	AAGATTGCCCAGAAAGCCCTGGAC
	Antisense	AACTGTCGCCACCAGAAAGCTGAG
NQO-1	Sense	GAAGAGCACTGATCGTACTGGC
	Antisense	GGATACTGAAAGTTCGCAGGG
GCLM	Sense	TGTCTTGGAATGCACTGTATCTC
	Antisense	CCCAGTAAGGCTGTAAATGCTC
β-Actin	Sense	CCTGAGGCACTCTTCCAGCCTT
	Antisense	TGCGGATGTCCACGTCACACTTC

4.4. Paracellular permeability of mineral ions and small molecules

Cells were cultured in Corning 6.5 mm Transwell plates with 0.4 μm pore polyester membrane inserts (Corning, NY, USA). TER was measured using a Millicell ERS-2 Volt-Ohm meter (MerckMillipore, Darmstadt, Germany). After subtracting the resistance of the blank filter, the values were represented as ohms × cm^2. In the glucose and AA flux assays, Hank's Balanced salt solution containing 10 mM glucose or Amino Acids Mixture Standard Solution (Fujifilm Wako Pure Chemicals) was added to the Transwell inserts. After incubation at 4°C for 30 min, the lower well solution was collected. The permeabilities of glucose and AAs were examined using a Glucose Assay Kit-WST (Dojindo Laboratories, Kumamoto, Japan) and a colorimetric L-Amino Acid Assay Kit (Cell Biolabs), respectively. The contents of each AA was analyzed using a LCMS-9030 mass spectrometer (Shimazu, Kyoto, Japan) as described previously [33] and represented as a percentage of negative siRNA.

4.5. Electron microscopy

Spheroids transfected with negative or CLDN1 siRNA were fixed with 2% paraformaldehyde and 2% glutaraldehyde in 0.1 M phosphate buffer. The preparation and electron microscopic analysis of samples

were carried out by Tokai Electron Microscopy (Nagoya, Japan) as described previously [16].

4.6. Immunocytochemistry

Spheroids transfected with negative or CLDN1 siRNA were fixed with 3.7% formaldehyde, and then cleared using CytoVista 3D Cell Culture Clearing reagent (Thermo Fisher Scientific, Rockford, IL, USA). The immunostaining and visualization of CLDN1 and ZO-1 were carried out as described previously [16].

4.7. Mitochondrial function and ROS production

Cells cultured in 96-well black plates were incubated with JC-1 iodide (Takara-Bio), MitoROS 580 (AAT Bioquest, Sunnyvale, CA, USA), or CellROX DeepRed (Thermo Fisher Scientific) at 37°C for 30 min. Then, the fluorescence images of JC-1, MitoROS 580, and CellROX were collected using a BZ-X810 (Keyence, Osaka, Japan), and represented as a percentage of siRNA for negative or 100% AAs. In the case of JC-1, the ratios of red to green fluorescence intensities were calculated.

4.8. Cell viability

Viabilities in 2D and 3D cultured cells were assessed using a Cell Counting Kit-8 (Dojindo Laboratories, Kumamoto, Japan) and CellTiter-Glo 3D Cell Viability Assay Kit (Promega, Madison, WI, USA), respectively. After subtracting background values, viability was represented as a percentage of the control cells.

4.9. Statistical analysis

Results are depicted as means ± standard error of the mean. Differences between groups were analyzed using one-way analysis of variance, and corrections for multiple comparison were made using Tukey's multiple comparison test. Comparisons between two groups were analyzed using Student's *t* test. Statistical analyses were conducted using KaleidaGraph version 5.0.3 software (Synergy Software, PA, USA). The statistical significance was set at $p < 0.05$.

Abbreviations

AA, amino acid; CLDN, claudin; DXR, doxorubicin; GCLM, glutamate cysteine ligase catalytic subunit; HIF-1, hypoxia-induced factor-1; HO-1, hemeoxygenase-1; Keap-1, Kelch-like ECH-associated protein 1; mTOR, mammalian target of rapamycin; mTORC1, mTOR complex 1; NQO-1, NAD(P)H:quinone oxidoreductase-1; Nrf2, nuclear factor-erythroid 2-related factor 2; NSCLC, non-small cell lung cancer; PCR, polymerase chain reaction; ROS, reactive oxygen species; SDS-PAGE, Sodium dodecyl sulfate polyacrylamide gel electrophoresis; TCA, tricarboxylic acid; TER, transepithelial electrical resistance; TJ, tight junction; ZO-1, zonula occludens-1; 2D, two-dimensional; 3D, three-dimensional

Declarations

Declaration of competing interest

The author declare that they have no conflicts of interest.

Author Contribution

R. K., A. Ito, S. H., H. E., H. N., Y. T., Y. M., and K. S. performed experiments and analyzed the data. Y. Y., S. E., and T. M. contributed to the experiment plan and discussion of the manuscript. A. Ikari contributed to supervision of the project, interpretation of data and writing the paper. All authors reviewed the results and approved the final version of the manuscript.

Acknowledgments

This work was supported in part by JSPS KAKENHI Grant Number 19H03373, and grants from the Takeda Science Foundation, Futaba Electronics Memorial Foundation, Kobayashi Foundation for Cancer Research, Koshiyama Research Foundation, Promotion of Cancer Research, Kobayashi Foundation, and Smoking Research Foundation (to A.I.).

Data Availability

The datasets used and/or analysed during the current study available from the corresponding author on reasonable request.

References

1. Farc, O. & Cristea, V. An overview of the tumor microenvironment, from cells to complex networks (Review). *Exp. Ther. Med.* **21**, 96, doi:10.3892/etm.2020.9528 (2021).
2. Yfantis, A. *et al.* Transcriptional Response to Hypoxia: The Role of HIF-1-Associated Co-Regulators. *Cells* **12**, doi:10.3390/cells12050798 (2023).
3. Taguchi, K. & Yamamoto, M. The KEAP1-NRF2 System in Cancer. *Front. Oncol.* **7**, 85, doi:10.3389/fonc.2017.00085 (2017).
4. Wibbe, N. & Ebnet, K. Cell Adhesion at the Tight Junctions: New Aspects and New Functions. *Cells* **12**, doi:10.3390/cells12232701 (2023).
5. Meoli, L. & Gunzel, D. The role of claudins in homeostasis. *Nat Rev Nephrol* **19**, 587-603, doi:10.1038/s41581-023-00731-y (2023).
6. Tepass, U. Claudin complexities at the apical junctional complex. *Nat. Cell Biol.* **5**, 595-597, doi:10.1038/ncb0703-595 (2003).
7. Adil, M. S., Narayanan, S. P. & Somanath, P. R. Cell-cell junctions: structure and regulation in physiology and pathology. *Tissue Barriers* **9**, 1848212, doi:10.1080/21688370.2020.1848212 (2021).

8. Krause, G. *et al.* Structure and function of claudins. *Biochim. Biophys. Acta* **1778**, 631-645, doi:10.1016/j.bbamem.2007.10.018 (2008).
9. Li, J. Dysregulated expression of claudins in cancer. *Oncol. Lett.* **22**, 641, doi:10.3892/ol.2021.12902 (2021).
10. Wang, D. W., Zhang, W. H., Danil, G., Yang, K. & Hu, J. K. The role and mechanism of claudins in cancer. *Front. Oncol.* **12**, 1051497, doi:10.3389/fonc.2022.1051497 (2022).
11. Ikari, A., Sato, T., Watanabe, R., Yamazaki, Y. & Sugatani, J. Increase in claudin-2 expression by an EGFR/MEK/ERK/c-Fos pathway in lung adenocarcinoma A549 cells. *Biochim. Biophys. Acta* **1823**, 1110-1118, doi:10.1016/j.bbamcr.2012.04.005 (2012).
12. Akizuki, R. *et al.* Decrease in paracellular permeability and chemosensitivity to doxorubicin by claudin-1 in spheroid culture models of human lung adenocarcinoma A549 cells. *Biochim. Biophys. Acta Mol. Cell Res.* **1865**, 769-780, doi:10.1016/j.bbamcr.2018.03.001 (2018).
13. Maruhashi, R. *et al.* Chrysin enhances anticancer drug-induced toxicity mediated by the reduction of claudin-1 and 11 expression in a spheroid culture model of lung squamous cell carcinoma cells. *Sci. Rep.* **9**, 13753, doi:10.1038/s41598-019-50276-z (2019).
14. Primeaux, M. *et al.* Claudin-1 interacts with EPHA2 to promote cancer stemness and chemoresistance in colorectal cancer. *Cancer Lett.* **579**, 216479, doi:10.1016/j.canlet.2023.216479 (2023).
15. Tong, H., Li, T., Qiu, W. & Zhu, Z. Claudin-1 silencing increases sensitivity of liver cancer HepG2 cells to 5-fluorouracil by inhibiting autophagy. *Oncol. Lett.* **18**, 5709-5716, doi:10.3892/ol.2019.10967 (2019).
16. Ito, A. *et al.* Elevation of Chemosensitivity of Lung Adenocarcinoma A549 Spheroid Cells by Claudin-2 Knockdown through Activation of Glucose Transport and Inhibition of Nrf2 Signal. *Int. J. Mol. Sci.* **22**, 6582, doi:10.3390/ijms22126582 (2021).
17. Pranzini, E., Pardella, E., Paoli, P., Fendt, S. M. & Taddei, M. L. Metabolic Reprogramming in Anticancer Drug Resistance: A Focus on Amino Acids. *Trends Cancer* **7**, 682-699, doi:10.1016/j.trecan.2021.02.004 (2021).
18. Furfaro, A. L. *et al.* The Nrf2/HO-1 Axis in Cancer Cell Growth and Chemoresistance. *Oxid. Med. Cell. Longev.* **2016**, 1958174, doi:10.1155/2016/1958174 (2016).
19. Scherz-Shouval, R., Shvets, E. & Elazar, Z. Oxidation as a post-translational modification that regulates autophagy. *Autophagy* **3**, 371-373, doi:10.4161/auto.4214 (2007).
20. Xue, D., Zhou, X. & Qiu, J. Emerging role of NRF2 in ROS-mediated tumor chemoresistance. *Biomed. Pharmacother.* **131**, 110676, doi:10.1016/j.biopha.2020.110676 (2020).
21. Zhang, J. *et al.* Review of the Correlation of LAT1 With Diseases: Mechanism and Treatment. *Front Chem* **8**, 564809, doi:10.3389/fchem.2020.564809 (2020).
22. Imai, H. *et al.* L-type amino acid transporter 1 expression is a prognostic marker in patients with surgically resected stage I non-small cell lung cancer. *Histopathology* **54**, 804-813, doi:10.1111/j.1365-2559.2009.03300.x (2009).

23. Kaira, K. *et al.* Relationship between LAT1 expression and response to platinum-based chemotherapy in non-small cell lung cancer patients with postoperative recurrence. *Anticancer Res.* **31**, 3775-3782 (2011).
24. Liu, Y. H. *et al.* L-Type Amino Acid Transporter 1 Regulates Cancer Stemness and the Expression of Programmed Cell Death 1 Ligand 1 in Lung Cancer Cells. *Int. J. Mol. Sci.* **22**, doi:10.3390/ijms222010955 (2021).
25. Sha, R., Zhang, J., Meng, F. & Zhaori, G. Gastric cancer metastasis-related NT5DC2 indicates unfavorable prognosis of patients. *Medicine (Baltimore)* **102**, e35030, doi:10.1097/MD.0000000000035030 (2023).
26. Chang, Q. *et al.* SLC41A3 Exhibits as a Carcinoma Biomarker and Promoter in Liver Hepatocellular Carcinoma. *Comput. Math. Methods Med.* **2021**, 8556888, doi:10.1155/2021/8556888 (2021).
27. Rii, J. *et al.* Functional analysis of LAT3 in prostate cancer: Its downstream target and relationship with androgen receptor. *Cancer Sci.* **112**, 3871-3883, doi:10.1111/cas.14991 (2021).
28. Cormerais, Y., Vucetic, M., Parks, S. K. & Pouyssegur, J. Amino Acid Transporters Are a Vital Focal Point in the Control of mTORC1 Signaling and Cancer. *Int. J. Mol. Sci.* **22**, doi:10.3390/ijms22010023 (2020).
29. Zhang, B. *et al.* Regulation of branched-chain amino acid metabolism by hypoxia-inducible factor in glioblastoma. *Cell. Mol. Life Sci.* **78**, 195-206, doi:10.1007/s00018-020-03483-1 (2021).
30. Matsuyama, R. *et al.* Up-regulation of L-type amino acid transporter 1 (LAT1) in cultured rat retinal capillary endothelial cells in response to glucose deprivation. *Drug Metab. Pharmacokinet.* **27**, 317-324, doi:10.2133/dmpk.dmpk-11-rg-122 (2012).
31. Valdovinos-Flores, C. *et al.* Systemic L-Buthionine -S-R-Sulfoximine Treatment Increases Plasma NGF and Upregulates L-cys/L-cys2 Transporter and gamma-Glutamylcysteine Ligase mRNAs Through the NGF/TrkA/Akt/Nrf2 Pathway in the Striatum. *Front. Cell. Neurosci.* **13**, 325, doi:10.3389/fncel.2019.00325 (2019).
32. Inai, T., Kobayashi, J. & Shibata, Y. Claudin-1 contributes to the epithelial barrier function in MDCK cells. *Eur. J. Cell Biol.* **78**, 849-855, doi:10.1016/S0171-9335(99)80086-7 (1999).
33. Okamoto, E. *et al.* Regulation of Paracellular Fluxes of Amino Acids by Claudin-8 in Normal Mouse Intestinal MCE301 Cells. *Nutrients* **15**, doi:10.3390/nu15061346 (2023).
34. Okamoto, E. *et al.* Increase in Paracellular Leakage of Amino Acids Mediated by Aging-Induced Reduction of Claudin-4 Expression. *J. Nutr.* **153**, 3360-3372, doi:10.1016/j.tjnut.2023.09.026 (2023).
35. Li, Z. & Zhang, H. Reprogramming of glucose, fatty acid and amino acid metabolism for cancer progression. *Cell. Mol. Life Sci.* **73**, 377-392, doi:10.1007/s00018-015-2070-4 (2016).
36. Ryoo, I. G. & Kwak, M. K. Regulatory crosstalk between the oxidative stress-related transcription factor Nfe2l2/Nrf2 and mitochondria. *Toxicol. Appl. Pharmacol.* **359**, 24-33, doi:10.1016/j.taap.2018.09.014 (2018).
37. Saito, Y. *et al.* Amino acid starvation culture condition sensitizes EGFR-expressing cancer cell lines to gefitinib-mediated cytotoxicity by inducing atypical necroptosis. *Int. J. Oncol.* **52**, 1165-1177,

doi:10.3892/ijo.2018.4282 (2018).

Figures

Figure 1

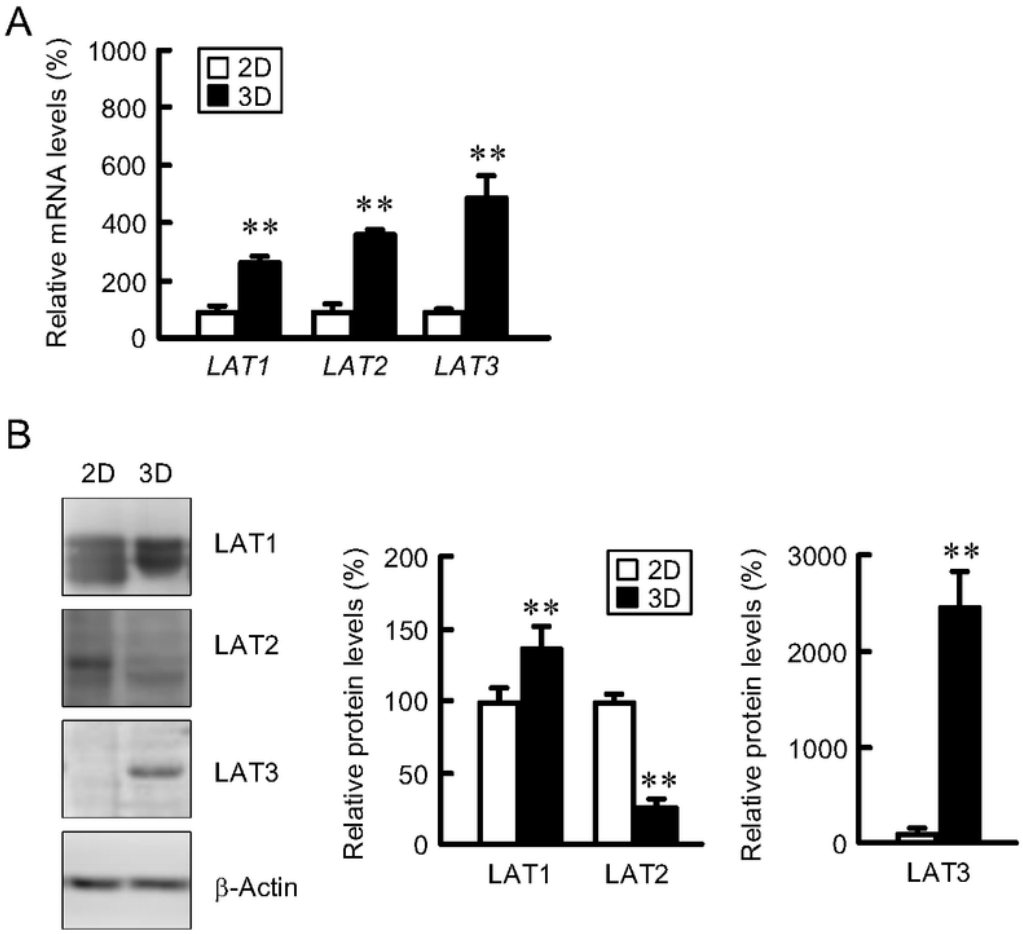

Figure 1

Increases in LAT1 and LAT3 expression levels in 3D cultures. A549 cells were cultured on flat dishes (2D) or96-well round-bottomed plates (3D) for 4 days. (A) The mRNA levels of *LAT1–3* were examined using quantitative real-time PCR and represented as a percentage of the 2D value. (B) The protein levels of LAT1–3 were examined using Westernblotting and represented as a percentage of the 2D value. n = 3–4.** $P < 0.01$ and * $P < 0.05$ compared with 2D.

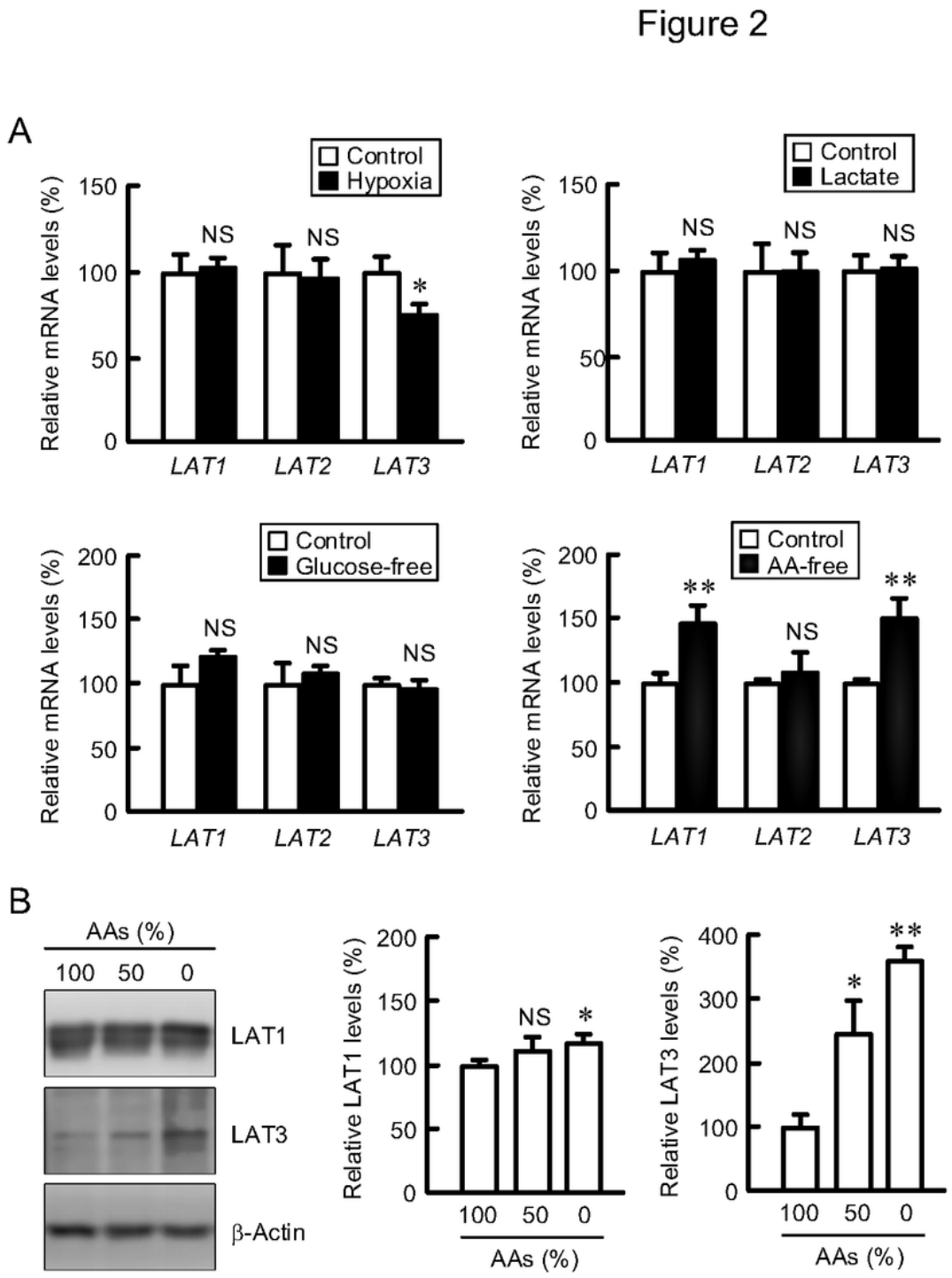

Figure 2

Increases in LAT1 and LAT3 expression levels with AA deficiency in 2D cultures. (A) A549 cells cultured in flat-bottomed dishes were exposed to hypoxia (0.5% O_2), high lactate (10 mM), glucose-free, or AA-free conditions for 6 h. The mRNA levels of *LAT1–3* were examined by quantitative real-time PCR and represented as a percentage of the control value. (B) A549 cells were exposed to AA deficiency conditions for 24 h. The protein levels of LAT1 and LAT3 were examined using Western blotting and represented as a percentage of the 100% AAs value. n = 3–4. ** $P < 0.01$, * $P < 0.05$, and ^{NS} $P > 0.05$ compared with control or 100% AAs.

Figure 3

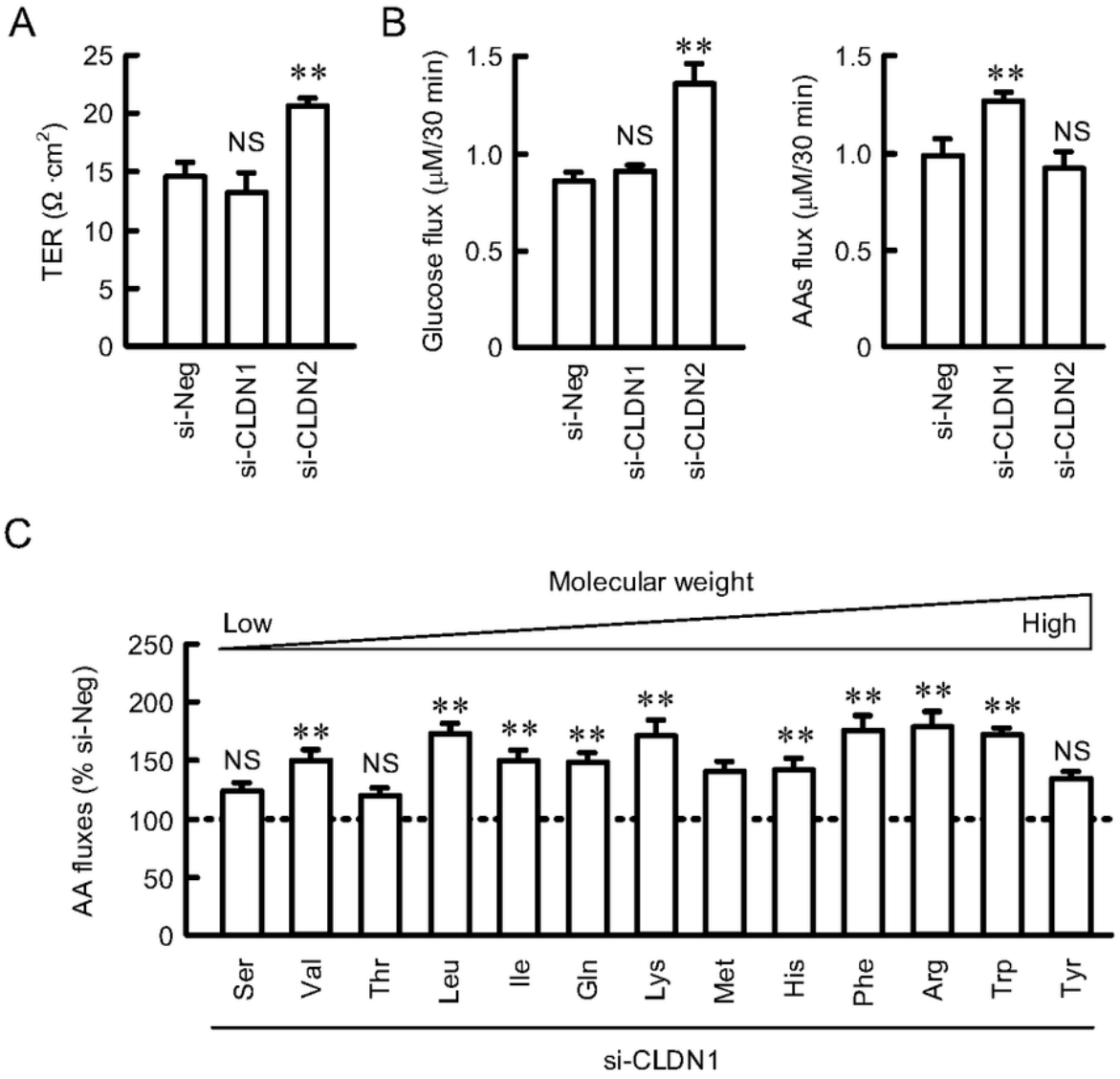

Figure 3

Increase in paracellular AA flux by CLDN1 silencing in 2D cultures. A549 cells cultured on Transwell inserts were transfected with negative control (si-Neg), CLDN1 (si-CLDN1), or CLDN2 (si-CLDN2) siRNAs. (A) TER was examined using a volt-ohm meter. (B) After addition of glucose or AAs to the upper chamber, the cells were incubated for 30 min at 4°C. The fluxes of glucose and AAs were measured using each assay kit. (C) The contents of AAs in the lower chamber were investigated using a liquid chromatography-

mass spectrometer and represented as a percentage of the negative siRNA value. n = 3–6. ** $P < 0.01$, * $P < 0.05$, and ^{NS} $P > 0.05$ compared with si-Neg.

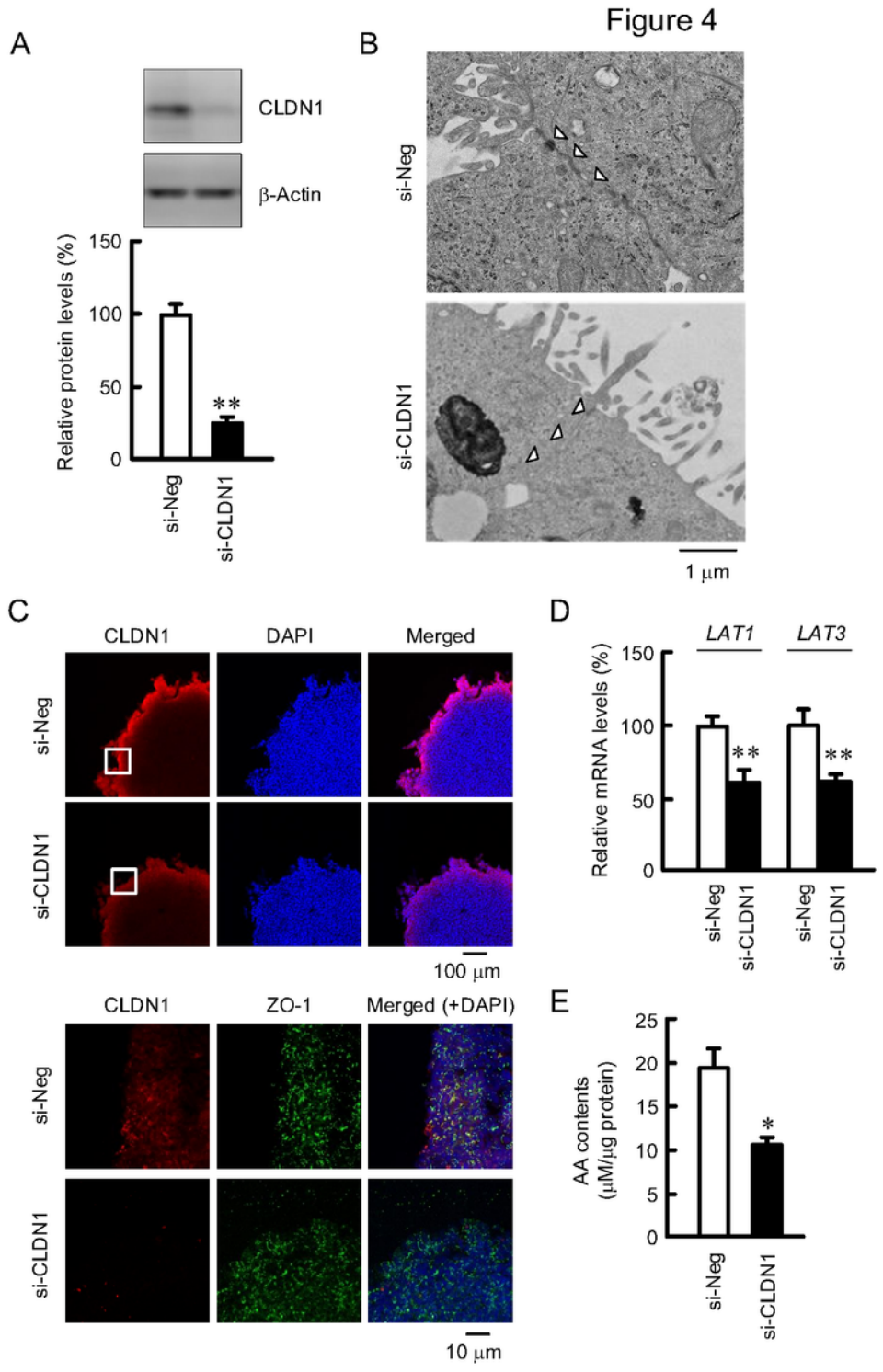

Figure 4

Effect of CLDN1 silencing on the structure of TJs in 3D cultures. A549 cells cultured in round-bottomed plates were transfected with negative control (si-Neg) or CLDN1 (si-CLDN1) siRNAs. (A) The protein levels

of CLDN1 were examined using Western blotting and represented as a percentage of the si-Neg value. (B) Transmission electron microscope images of the outer layer of spheroids. The kissing points are indicated with arrowheads. (C) After clearing using CytoVista 3D Cell Culture Clearing reagent, the cells were immunostained with rabbit anti-CLDN1 primary antibodies, mouse anti-ZO-1 primary antibodies, AlexaFluor-488 anti-mouse IgG, AlexaFluor-555 anti-rabbit IgG, and DAPI. Fluorescence images were collected using an LSM700 confocal microscope. Lower panels show enlarged images of the regions marked with a square in the upper panels. Scale bar indicates 100 μm. (D) The mRNA levels of *LAT1*and *LAT3* were examined using quantitative real-time PCR and represented as a percentage of the si-Neg value. (D) The AA contents in spheroids were investigated using an ELISA kit. n = 3–6. ** $P < 0.01$ and * $P < 0.05$ compared with si-Neg.

Figure 5

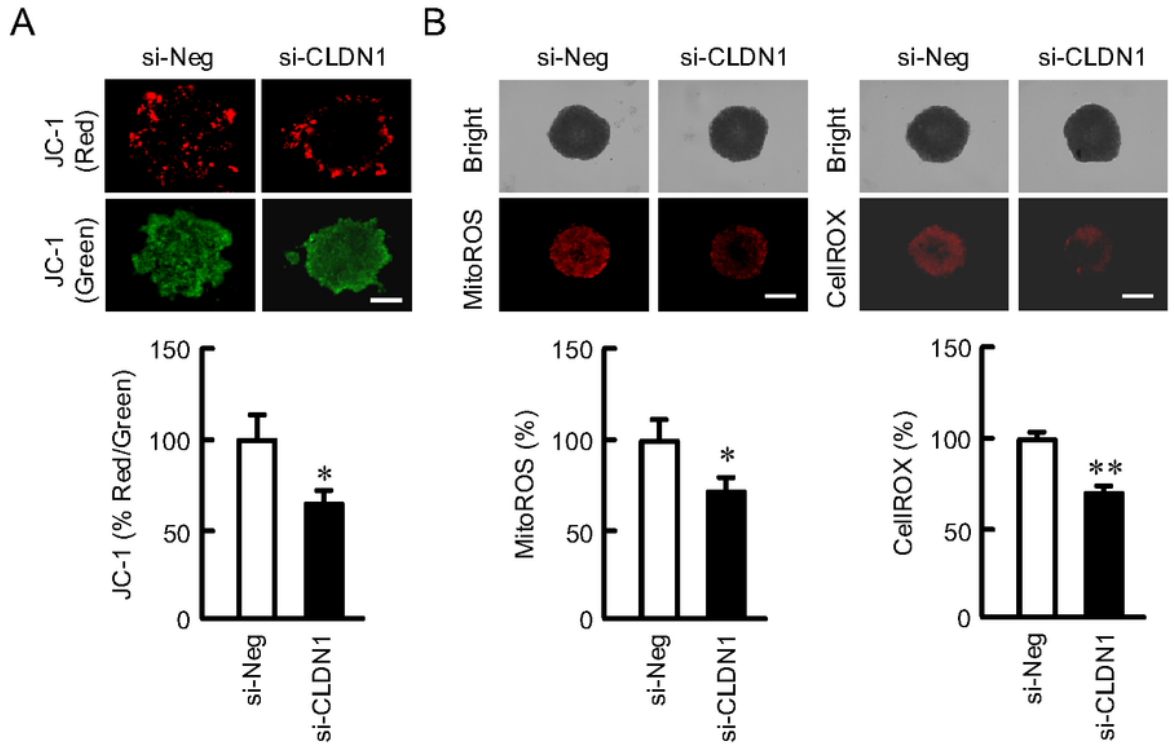

Figure 5

Effect of CLDN1 silencing on mitochondrial function in 3D cultures. A549 cells transfected with negative control (si-Neg) or CLDN1 (si-CLDN1) siRNAs were cultured in 96-well round-bottomed plates for 4 days. (A) Mitochondrial ROS production was examined using JC-1, and the ratios of red and green fluorescence was calculated by ImageJ. (B) Mitochondrial and cytosolic ROS production was examined using MitoROS 580 and CellROX, respectively. Fluorescence images were collected using an LSM700 confocal

microscope. The fluorescence intensity was measured using ImageJ and represented as a percentage of the si-Neg value. n = 6–8.** $P < 0.01$ and * $P < 0.05$compared with si-Neg.

Figure 6

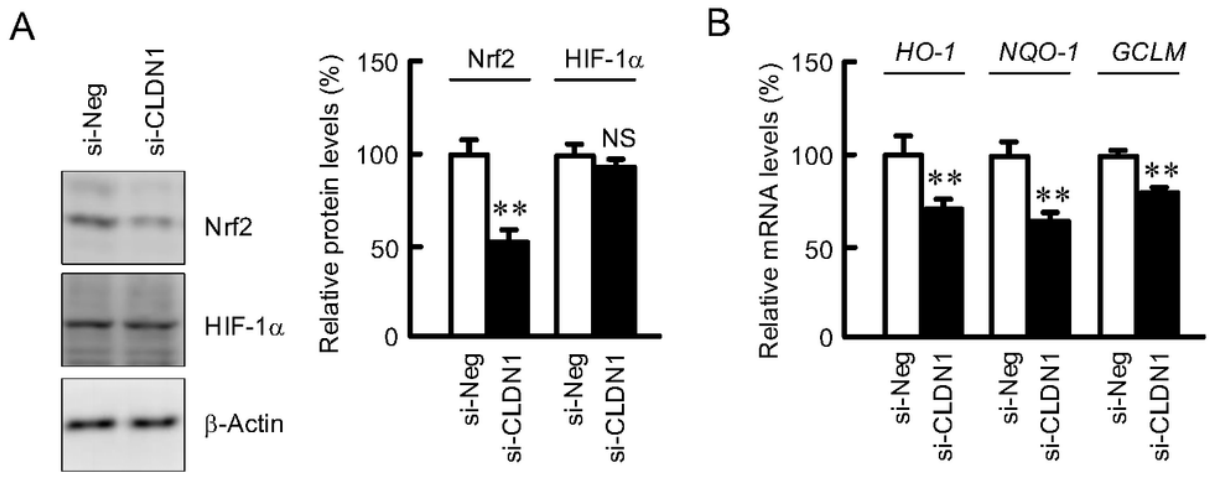

Figure 6

Decrease in the expression of Nrf2 and Nrf2-related genes by CLDN1 silencing in 3D cultures. A549 cells transfected with negative control (si-Neg) or CLDN1 (si-CLDN1) siRNAs were cultured in 96-well round-bottomed plates for 4 days. (A) The protein levels of Nrf2 and HIF-1α were examined using Western blotting and represented as a percentage of the si-Neg value. (B) mRNA levels of *HO-1*,*NQO-1*, and *GCLM* were examined using quantitative real-time PCR and represented as a percentage of the si-Neg value. n = 3. ** $P < 0.01$ and NS $P > 0.05$ compared with si-Neg.

Figure 7

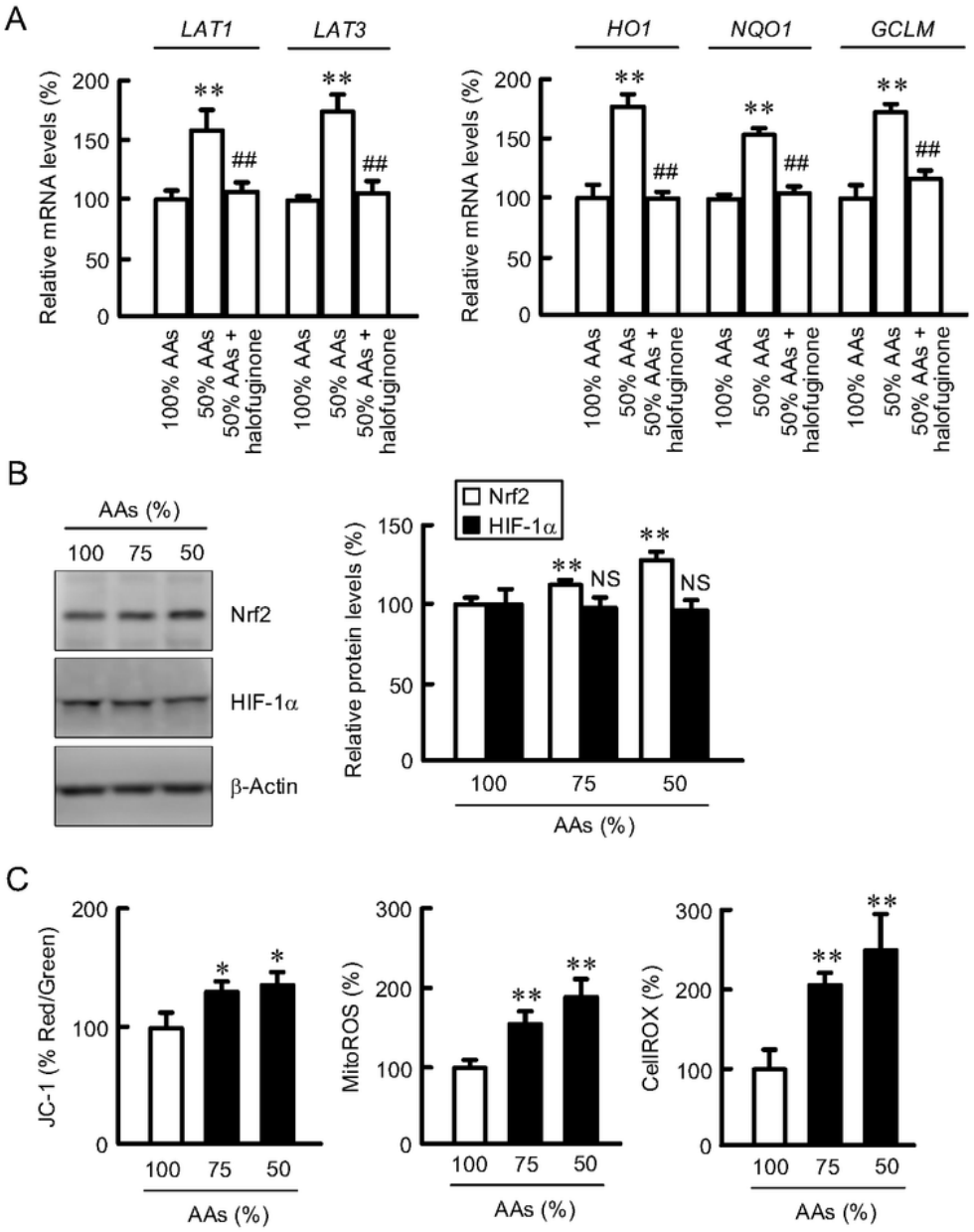

Figure 7

Effects of AA deficiency on Nrf2 expression and mitochondrial function in 2D cultures. (A) A549 cells cultured in flat-bottomed dishes were incubated with 100%, 75%, or 50% AA-containing medium for 6 h in the presence or absence of 10 nM halofuginone. The mRNA levels of *LAT1, LAT3, HO-1*, *NQO-1*, and *GCLM* were examined using quantitative real-time PCR and represented as a percentage of the 100% AAs value. (B) A549 cells cultured in flat-bottomed dishes were incubated with 100%, 75%, or 50% AA-

containing medium for 24 h. The protein levels of Nrf2 and HIF-1α were examined using Western blotting and represented as a percentage of the 100% AAs value. (C) A549 cells cultured in 96-well plates were incubated with 100%, 75%, or 50% AA-containing medium for 6 h. The mitochondrial membrane potential, mitochondrial ROS production, and cytosolic ROS production were examined using specific fluorescent probes, and the relative fluorescence intensities were represented as a percentage of the 100% AAs value. n = 3–6.** $P < 0.01$, * $P < 0.05$, and NS $P > 0.05$ compared with 100% AAs.

Figure 8

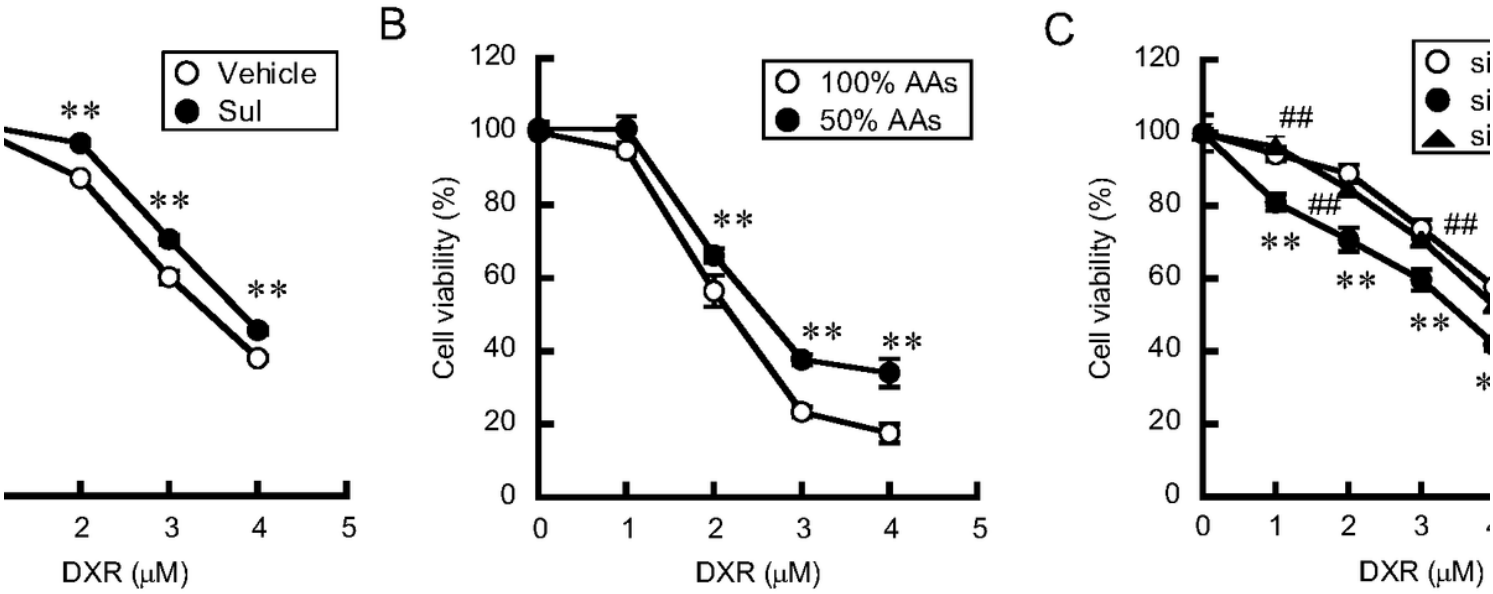

Figure 8

Inhibition of CLDN1 knockdown-induced chemosensitization by sulforaphane. (A) A549 cells cultured in flat-bottomed dishes were preincubated with 10 mM sulforaphane (Sul) or 50% AA-containing medium for 24 h. Then, the cells were incubated with doxorubicin (DXR) for 24 h, followed by assessment of cell viability. (C) A549 cells transfected with negative control (si-Neg) or CLDN1 (si-CLDN1) siRNA were cultured in 96-well round-bottomed plates for 3 days. Then, the cells were incubated in the absence or presence of 10 mM Sul and DXR for 24 h, followed by assessment of cell viability using a CellTiter-Glo 3D Cell Viability Assay Kit. n = 4–6. ** $P < 0.01$ and * $P < 0.05$ compared with vehicle, 100% AAs, or si-Neg values. ## $P < 0.01$ compared with si-CLDN1 alone.

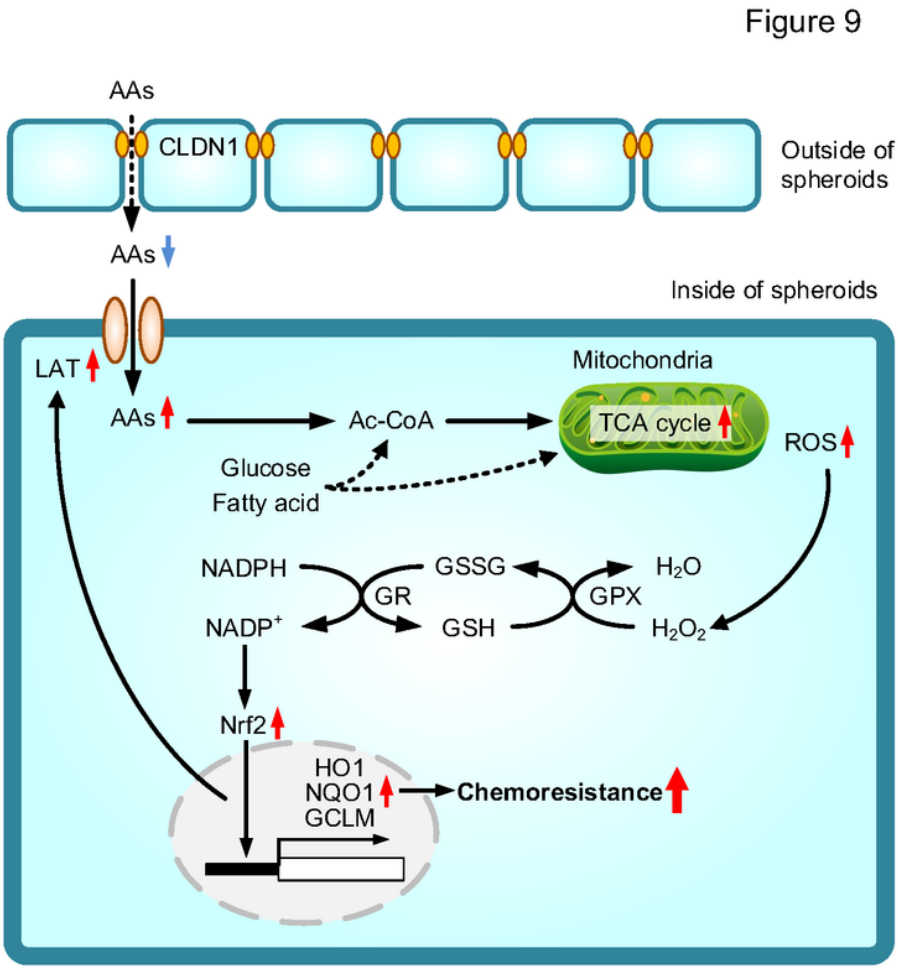

Figure 9

A putative model of CLDN1-induced chemoresistance. The cells expressing CLDN1 on the outside of spheroids inhibit paracellular influx of AAs. AA deprivation enhanced LAT expression, mitochondrial activity, TCA cycle, and ROS generation. Oxidative stress confers chemoresistance mediated by the activation of Nrf2 signalling.